Clumped-isotope-derived climate trends leading up to the end-Cretaceous mass extinction in northwest Europe

Heidi E. O'Hora[1], B. Sierra V. Petersen[1], Johan Vellekoop[2,3], Matthew M. Jones[1], Serena R. Scholz[1]

[1]Department of Earth and Environmental Sciences, University of Michigan, Ann Arbor, MI 48104, USA
5 [2]Analytical, Environmental, and Geo-Chemistry, Vrije Universiteit Brussel, B-1050 Brussels, Belgium
[3]Department of Earth and Environmental Sciences, KU Leuven, 3000 Leuven, Belgium

Correspondence to: Heidi E. O'Hora (ohora@umich.edu)

Abstract. Paleotemperature reconstructions linked to Deccan traps volcanic greenhouse gas emissions and associated feedbacks in the lead-up to the end-Cretaceous meteorite impact and extinction document local and global climate trends
10 during a key interval of geologic history. Here, we present a new clumped-isotope-based paleotemperature record derived from fossil bivalves from the Maastrichtian type region, in southeast Netherlands and northeast Belgium. Clumped isotope data documents a mean temperature of 19.2 ± 3.8 °C, consistent with other Maastrichtian temperature estimates, and an average seawater $\delta^{18}O$ value of -0.3 ± 0.9‰ VSMOW for the region during the latest Cretaceous (67.1–66.0 Ma). A notable temperature increase at ~66.4 Ma is interpreted to be a regional manifestation of the globally-defined Late Maastrichtian
15 Warming Event, linking Deccan Traps volcanic CO_2 emissions prior to the end-Cretaceous extinction to climate change in the Maastricht region. Fluctuating seawater $\delta^{18}O$ values coinciding with temperature changes suggest alternating influences of warm, salty southern-sourced waters and cooler, fresher northern-sourced waters from the Arctic Ocean. This new paleotemperature record contributes to the understanding of regional and global climate response to large-scale volcanism and ocean circulation changes leading up to a catastrophic mass extinction.

20 **1 Introduction**

During the Late Maastrichtian, greenhouse gas emissions from the emplacement of the vast Deccan Traps large igneous province (LIP) on the Indian subcontinent resulted in global warming (see Hull et al., 2020 and references therein). This warming event (termed the Late Maastrichtian Warm Event or LMWE; Woelders et al., 2018) has been observed in multiple locations and has been dated to approximately coincide with the onset of major Deccan volcanism (66.413 ± 0.067 Ma;
25 Sprain et al., 2019). Anomalous mercury concentrations in sediments (e.g., Font et al., 2016; Sial et al., 2016; Percival et al., 2018; Zhao et al., 2021) and fossil shells (Meyer et al., 2019) link the warming to a volcanic source, and modeling of the climate impacts of hypothesized volcanic CO_2 and Hg emissions result in warming consistent with observations (Tobin et al., 2017; Fendley et al., 2019; Nava et al., 2021).

30   Prior to the LMWE, global climate was in a "cool greenhouse" state (Scotese, 2021), with a small ice cap possible in Antarctica as indicated by models (Miller et al., 2005; Ladant and Donnadieu, 2016), sea-ice-indicating dinoflagellate cysts (Bowman et al., 2013), and coastal Antarctic temperatures near the freezing point (Petersen et al., 2016a). The LMWE may have caused these ice caps to melt (Bowman et al., 2013; Petersen et al, 2016a) and, subsequently, global sea level to rise. This is potentially visible in the global sea level curve of Haq (2014), but the resolution of this sea level record is too coarse

35   to directly link cycles to the short-term LMWE.

After the LMWE, climate cooled again gradually, potentially due to silicate weathering feedbacks (Petersen et al., 2016a; Tobin et al., 2017), before being thrown into upheaval by the arrival of the Chicxulub meteorite impact, defining the Cretaceous-Paleogene (K-Pg) boundary (Molina et al., 2006). Ejecta from the impact covered the planet and resulted in a

40   short-lived "impact winter" event (Vellekoop et al., 2014; Vellekoop et al., 2016). Taken together, Deccan Traps volcanism and associated feedbacks and the Chicxulub bolide impact create a complex record of paleoenvironmental disturbances through the end-Cretaceous, ultimately leading to the rapid extinction of ~70 % of species on Earth (Schulte et al., 2010).

Previous studies have reconstructed Maastrichtian marine temperatures at sites around the globe using several different

45   proxies including $\delta^{18}O$ of foraminifera, molluscs, tooth enamel, and bulk carbonate material (e.g., Pucéat et al., 2007; Tobin et al., 2012; Hull et al., 2020), TEX_{86} measurements (e.g., Vellekoop et al., 2016; Woelders et al., 2017), Mg/Ca ratios (e.g., Woelders et al., 2018), and clumped isotope thermometry (Dennis et al., 2013; Tobin et al., 2014; Petersen et al., 2016a; Petersen et al., 2016b, Meyer et al., 2018; Zhang et al., 2018; Meyer et al., 2019; Tagliavento et al., 2019) (Table S1). Taken together, these records clearly show a late Maastrichtian warming. However, at any given site, local ocean temperatures are

50   influenced not only by global trends, but by local changes in ocean circulation, sea level, upwelling, runoff, etc. (changes which may themselves by driven indirectly by global climate change, e.g., sea level rise due to melting of the Antarctic ice caps during the LWME). Therefore, it is important to consider the local paleogeographic context when interpreting paleoclimate trends during this tumultuous period.

55   Here, we produce a new climate record for a site in northwest Europe using the clumped and stable isotopic composition of bivalve fossils to better constrain the magnitude of climate change and possible ocean circulation fluctuations during this key geologic transition interval. We focus on the Maastrichtian type area (Jagt and Jagt-Yazykova, 2012) in the Belgium-Netherlands border region near Maastricht, Netherlands. The reconstructed paleogeography of this locality—a shallow epicontinental sea surrounded by several low-lying landmasses (Fig. 1a)—makes this site sensitive not only to global climate

60   changes, but to local variations in sea level and ocean circulation. We interpret our data in terms of previously described and modeled estimates for local, regional, and global climate changes during this time. Our study adds to a growing body of literature documenting the impacts of volcanism and ocean circulation on climate, especially leading up to the K-Pg extinction.
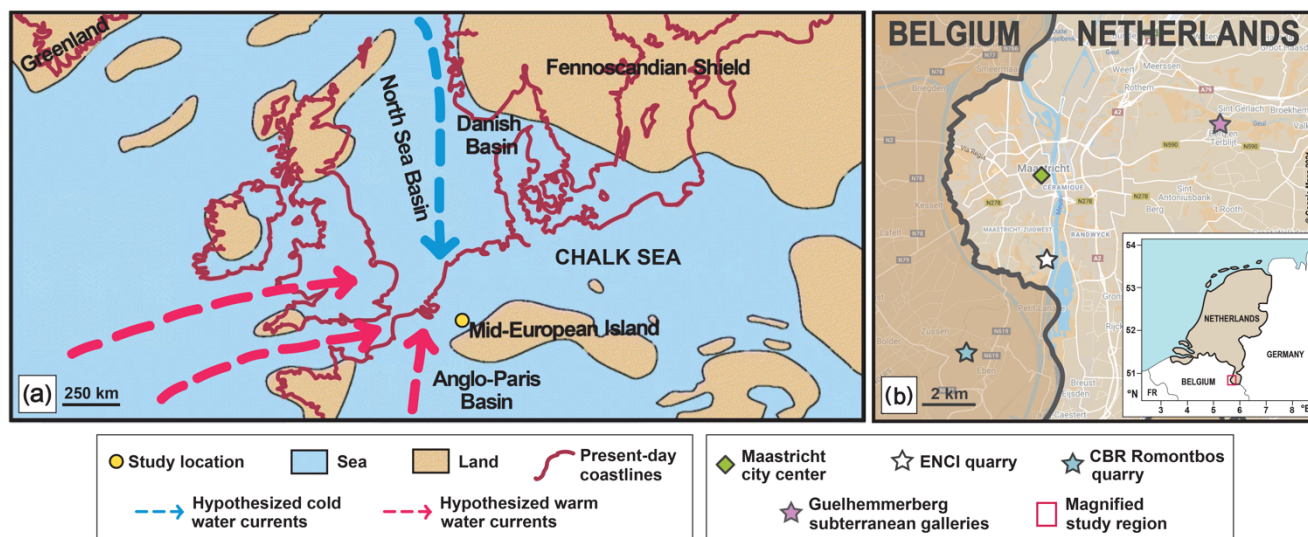
Figure 1: Paleogeography and sample localities for this study. (a) Late Cretaceous paleogeographic reconstruction of Europe and surrounding regions modified from Engelke et al. (2017) with the Maastricht region study location and hypothesized cold and warm water currents marked. (b) A modern-day map (from © Google Maps 2021) of the Maastricht region, located at the southernmost tip of the Netherlands (see inset), shows the relative position of the ENCI Quarry, Geulhemmerberg subterranean galleries, and CBR Romontbos quarry sampling localities to each other and to the city center of Maastricht.

2 Locality and Sample Collection

Shell specimens were collected from three locations in the Liège-Maastricht region of northeastern Belgium and southeastern Netherlands: the Maastrichtian type section at ENCI quarry, the CBR Romontbos quarry, and the K-Pg boundary (KPB) section at the Geulhemmerberg subterranean galleries (GSGs) (Jagt and Jagt-Yazykova, 2012) (Fig. 1b). The ENCI quarry is located ~3.3 km south of the city of Maastricht in South Limburg, Netherlands (Fig. 1b). Maastrichtian-aged strata at this location include the Gulpen Formation (~67.1–78.9 Ma) overlain by the Maastricht Formation (~66.0–66.8 Ma) (Vellekoop et al., in prep.), the latter of which was sampled for this study of the uppermost Maastrichtian Stage. At this location, the stratigraphically highest exposure of the Maastricht Formation in the Meerssen Member predates the KPB by less than 100 kyr (Keutgen, 2018). The CBR Romontbos quarry is located ~4 km to the southwest of ENCI quarry, near Eben Emael, Liège, Belgium (Fig. 1b). The Maastricht Formation is also exposed at this outcrop, and samples were correlated to align with the Maastricht Formation at ENCI quarry. In order to study the boundary interval itself, we also include a specimen from the nearby GSGs, which lie stratigraphically above the ENCI quarry and preserves the uppermost section of the Meerssen Member, including the K-Pg boundary interval. These subterranean galleries are located ~7 km east-northeast of ENCI quarry (Fig. 1b). There is an undetermined amount of missing time that is not exposed in either section (as indicated in Figure 2), which is constrained to less than 100 kyr.
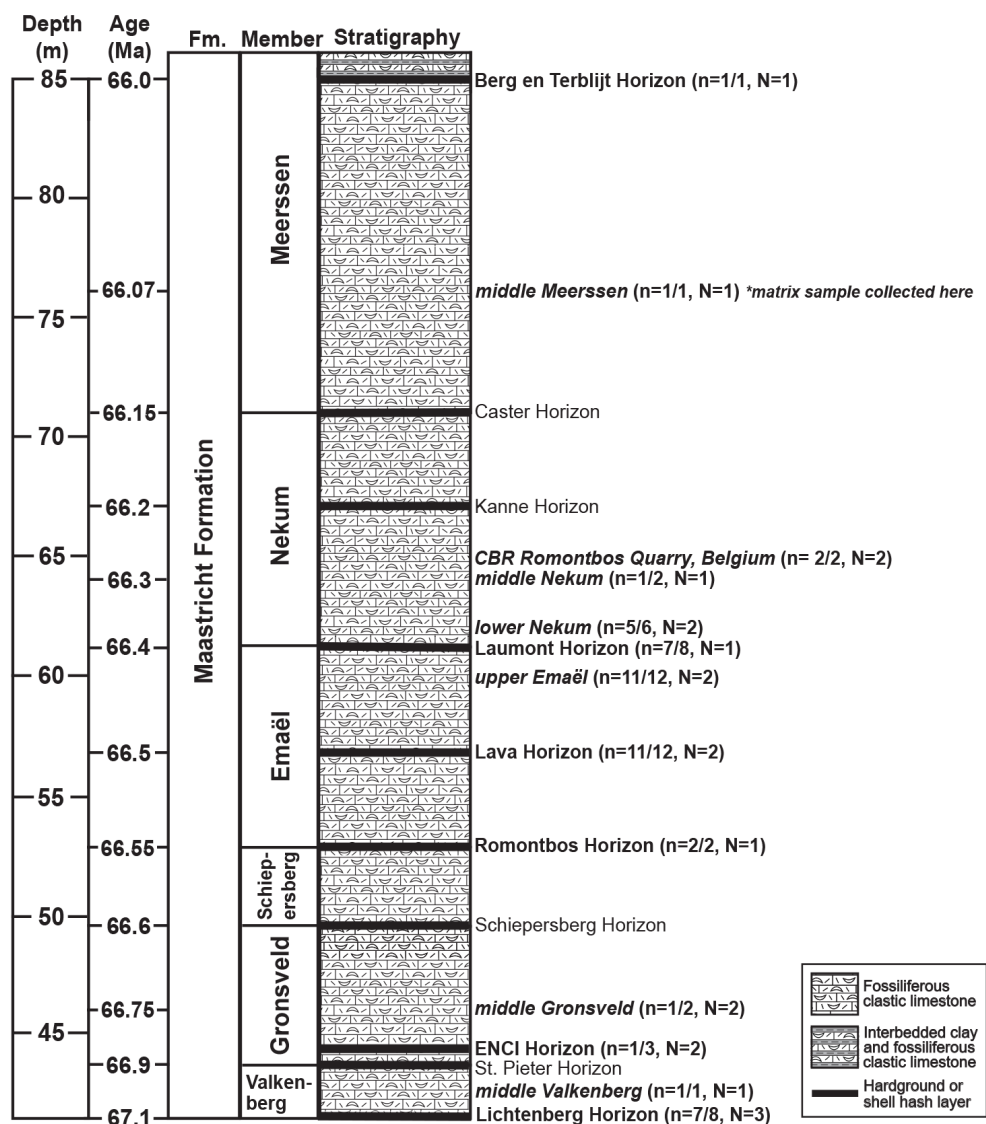
Figure 2: Composite stratigraphic section through the Maastricht Formation at ENCI quarry and Geulhemmerberg subterranean galleries. Number of specimens collected from horizons or intervals is listed on the right along with the number that passed diagenesis screening and the number of good specimens analyzed for clumped isotopes and interpreted here (n=passed/collected, N=clumped). Age model from Vellekoop et al. (in prep.). Berg en Terblijt Horizon assigned an age of 66.0 (Clyde et al., 2016; Sprain et al., 2018) and a depth of 85 m via correlation to ENCI quarry outcrop. Two specimens from the Nekum Member of the CBR Romontbos quarry in nearby Liège Province, Belgium were correlated to this section and are labeled therein.

At ENCI quarry, the Maastricht Formation consists predominantly of bioclastic calcarenites and calcirudites that coarsen upward, indicative of a gradual increase in hydrodynamic energy in the depositional environment (Schiøler, 1997; Vellekoop et al., in prep.). The lower part of the formation consists of fining-upward bioclastic silt and fine-grained sand, while the upper portion consists of fining-upward bioclastic sand beds (Schiøler, 1997; Vellekoop et al., in prep). Crossbedding and

crosslamination are present in the lower parts of the Emaël, Nekum, and Meerssen Members (Zijlstra, 1994; Schiøler, 1997).
100 This formation is interpreted to represent a shallow marine carbonate shelf that was subjected to fluctuating sea level and erosion (Schiøler, 1997). Prominent, fossiliferous horizons have been identified within the facies in this region (Felder, 1975; Zijlstra, 1988; Schiøler, 1997), including nine horizons in the Maastricht Formation at ENCI quarry (Fig. 2). Fossil shell specimens were collected from five of these horizons (Lichtenberg, ENCI, Romontbos, Lava, and Laumont), as well as from the top of the Emaël Member, the basal and middle intervals of the Nekum Member, and the basal interval of the Meerssen
105 Member (Fig. 2).

In the GSGs, the uppermost Maastrichtian interval of the Meerssen Member is capped by the fossiliferous Berg en Terblijt Horizon, thought to mark the K-Pg extinction event and end of the Cretaceous Period (Smit and Brinkhuis, 1996). Directly above this horizon, interbedded layers of Danian-aged non-fossiliferous clay and fossiliferous limestone represent the KPB
110 interval of the Maastricht Formation (Smit and Brinkhuis, 1996; Vellekoop et al., 2020) (Fig. 2). The specimen collected from the GSGs came from a shell hash layer directly above the Berg en Terblijt Horizon and below fossil-free clays. This fossil assemblage is interpreted to be a tsunami deposit (Smit, 1999), and the specimen was likely alive right around the KPB and was deposited in this layer postmortem via the tsunami or other storm reworking. It was therefore assigned an age of 66.0 Ma (Clyde et al., 2016; Sprain et al., 2018).
115

Fossil shell specimens collected from the Maastricht Formation at the ENCI quarry, the CBR Romontbos quarry, and the GSGs included 60 bivalve specimens representing ten identified taxa of oysters, scallops, and clams (*Pseudoptera* sp*., Pycnodonte vesicularis, Acutostrea uncinella, Gryphaeostrea canaliculate, Agerostrea ungulata, Entolium membranaceum, Pinna* sp*., Neithea regularis,Ceratostreon* sp*.,* and *Rastellum* sp.), as well as four unidentified oysters and five unidentified
120 bivalves. In these units, all biogenic aragonite has dissolved, leaving behind hollowed molds. All taxa sampled here originally formed calcite shells.

Taxa-specific clumped isotope vital effects in bivalves are considered uncommon, based on studies of modern bivalve taxa (Eagle et al., 2013; Henkes et al., 2013; Came et al., 2014). Therefore, well-preserved specimens are expected to faithfully
125 record paleoenvironmental temperatures. Water depths for this location are estimated to be less than 20 m at all times, and often shallower (Hart et al., 2016), so reconstructed mean annual water temperatures are interpreted to approximate mean annual surface air temperatures. All measured specimens were sessile epifaunal suspension feeders and are assumed to have avoided significant lateral postmortem transport, apart from the specimen from the KPB tsunami horizon. Additionally, bulk matrix material from the Meerssen Member was analyzed for comparison to fossil shells, in order to assess the potential for
130 diagenetic alteration of samples.

3 Methods

3.1 Sample preparation

Carbonate samples were collected from the 60 fossil shell specimens by either hand-drilling or manual crushing in a mortar and pestle after removal of matrix material. One sample of matrix from the Meerssen Member was powdered and analyzed

135   for comparison to co-occurring fossil shells. The sample powders were divided for trace element analysis and isotopic analysis. Fragments of some shell specimens were mounted for SEM observation to assess their preservation state.

3.2 Preservation assessment (SEM)

The isotopic composition of fossil shells is susceptible to post-depositional alteration via recrystallization, which can skew interpreted formation temperatures (Brand and Morrison 1987). All fossil shells collected for this study were screened for

140   recrystallization using a combination of scanning electron microscopy (SEM) imaging and trace element detection methods. SEM imagery was performed on a JEOL JSM-7800FLV field-emission SEM in the Robert B. Mitchell Electron Microbeam Analysis Lab at the University of Michigan Ann Arbor. Of the 60 shell specimens, a subset of 17 specimens (with at least one representing each analyzed horizon) were selected for SEM imagery of the shell microstructure and inspection for indications of dissolution and/or presence of secondary calcite growth.

145   3.3 Preservation assessment (trace elements)

Elevated levels of trace elements (Mn and Fe especially) in calcitic fossil material may indicate diagenesis/recrystallization of the calcite (Land, 1967; Möller and Kubanek, 1976; Brand and Morrison, 1987; de Winter et al., 2018). All 61 samples were analyzed in the Michigan Elemental Analysis Laboratory at the University of Michigan for Mn and Fe concentrations using a Thermo Scientific Quadrupole-ICP-MS (iCAP Q) equipped with an Elemental Scientific PrepFAST 2 Automation

150   System. KED mode (He gas) was utilized for all isotopes. All samples were analyzed in 2% HNO_3 (w/v) (Optima grade), and sensitivity drift was corrected for with standard-sample bracketing methods.

3.4 Stable isotope analysis

Powders drilled or crushed from 60 shell specimens and one matrix sample were analyzed for oxygen ($\delta^{18}O$) and carbon ($\delta^{13}C$) stable isotope compositions. Of all the shells, 39 were analyzed using a Thermo-Finnigan Kiel IV automated

155   carbonate device coupled to a MAT 253 gas source dual inlet mass spectrometer in the University of Michigan Stable Isotope Laboratory. Data were corrected for acid fractionation and normalized to the VPDB scale using NBS-18 and NBS-19 standards. Accuracy and precision were maintained at better than ±0.1 ‰ for both carbon and oxygen. The remaining 22 samples (21 shells, one matrix) were analyzed for $\delta^{18}O$ and $\delta^{13}C$ in conjunction with clumped isotope analysis in the University of Michigan Stable and Clumped Isotopes for Paleoclimatology and Paleoceanography (SCIPP) Laboratory (see

160   below).

3.5 Clumped isotope analysis

Powders drilled or crushed from 15 shell specimens and one matrix sample were measured for clumped isotopic composition (Δ_{47}) in the University of Michigan SCIPP Lab between 2016–2020 using a Thermo-Finnigan MAT 253 dual inlet mass spectrometer and a manual sample preparation device described by Defliese et al. (2015), with updates to Porapak temperature as outlined by Petersen et al. (2016c). This measurement simultaneously acquires $\delta^{13}C$ and $\delta^{18}O$ of CO_2 gas and Δ_{47}, which is a function of temperature (Eiler, 2011). Raw voltages were converted to isotopic values using IUPAC/Brand parameters following Petersen et al. (2019). Raw Δ_{47} values were placed in the absolute reference frame of Dennis et al. (2011), using theoretical equilibrium values for heated (1000 °C) and water-equilibrated (25 °C) standard gases (0.0266 and 0.9198, respectively) and the 75 °C acid fractionation factor of +0.072 ‰ from Petersen et al. (2019). $\delta^{18}O$ of carbonate ($\delta^{18}O_{carb}$) was calculated from $\delta^{18}O$ of evolved CO_2 using an empirical acid fractionation factor defined using in-house carbonate standards independently calibrated to NBS-18 and NBS-19.

Powders from six more shells were analyzed in the SCIPP lab in 2021 using a Nu Perspective IRMS connected to a NuCarb device. This sample preparation device reacts samples in individual vials at 70 °C and follows an automated routine to clean and analyze CO_2. Raw Δ_{47} values were calculated from raw voltages using an R code modeled off the one in Petersen et al. (2019), adjusted to accommodate data formats from the Nu instrument. Isotopic values were converted into the absolute reference frame based on the measurements of four ETH standards with Δ_{47} values defined by the Intercarb project (Bernasconi et al., 2021). Data was corrected using an acid fractionation factor of +0.066 for 70 °C from Petersen et al. (2019).

Final, acid-corrected Δ_{47} values from both measurement periods were converted to temperature using the composite calibration of synthetic carbonates from Petersen et al. (2019) [$Temp = (0.0383*10^6)/(\Delta_{47}–0.258)–273.15$]. For better direct comparison with the previously published clumped isotope data from Meyer et al. (2018; 2019), the published data were reprocessed using IUPAC/Brand parameters, instead of the previously used Santrock/Gonfiantini parameters, and converted to temperature using the same procedure as our new data.

Seawater $\delta^{18}O$ ($\delta^{18}O_{sw}$) was calculated for these 21 shell specimens using measured $\delta^{18}O_{carb}$ and Δ_{47}-derived temperatures and the calcite-water relationship described by Kim and O'Neil (1997). All $\delta^{18}O_{sw}$ values are reported on the VSMOW scale.

3.6 Age model

Ages for all stratigraphic horizons, lithostratigraphic boundaries, and specimens were determined by updating the Keutgen (2018) age model using known biostratigraphic markers and bulk carbon isotope data (Vellekoop et al., in prep.). All ages

have an uncertainty of ± 0.05 Ma, with the exception of the Lichtenberg Horizon (uncertainty of ± 0.2 Ma) and the Berg en Terblijt Horizon (uncertainty of ± 0.01 Ma).

4 Results

195 ### 4.1 Preservation and sample screening

Isotopic compositions may be affected by dissolution, recrystallization/replacement of shell material in a diagenetic environment, or overgrowth of secondary material. Clumped isotopic compositions may additionally be affected by solid-state bond reordering, which reduces heavy isotope pair bonding in the crystal lattice and overprints the original recorded temperature without any mass transfer. Bond reordering can occur if samples are heated above 100–150 °C (Henkes et al.,
200 2014; Winkelstern and Lohmann, 2016), such as during burial. This process is invisible to our direct screening methods (e.g., SEM, trace elements) but can be constrained from estimates of maximum burial depth/temperature.

Regional geologic evidence suggests a relatively shallow burial history for these strata. In the southern Netherlands, the Roer Valley Graben contains several basin-wide unconformities dated to the Late Cretaceous and middle Paleocene that signify
205 two basin inversions, leaving the Maastrichtian and Danian strata relatively undisturbed (Luijendijk et al., 2011 and references therein). Outstandingly well-preserved mosasaur skeletons and hollow aragonitic molds in the Maastricht Formation further indicate a lack of burial or significant diagenetic fluid flow during this time (Dortangs et al., 2002; Jagt et al., 2016). Overall, these burial conditions are not expected to result in bond reordering in any samples.

210 Evidence of dissolution of original shell material and/or overgrowth of secondary, diagenetic calcite are observable in SEM textures and/or trace element concentrations. In the 60 shell specimens tested for trace elements, Mn ranges from 17–210 ppm, and Fe ranges from 96–7151 ppm. The matrix sample exhibits 60 ppm Mn and 664 ppm Fe. By aligning the SEM observations with the trace element results, threshold values of 100 ppm and 2500 ppm were selected for Mn and Fe, respectively. These thresholds screen out all but two shell samples that showed secondary growth under SEM, while keeping
215 all samples that exhibited original material (Fig. 3). These thresholds are more conservative than those proposed by other studies (Morrison and Brand, 1987; Voigt et al., 2003; Ullmann et al., 2013, de Winter et al., 2018), but, in total, still only result in the removal of nine specimens out of 60, which are not included in discussions of isotopic compositions below. Isotopic evidence supports that these are conservative trace element thresholds. Despite being excluded based on SEM and trace element results, the isotopic values of excluded samples were not substantially different than other shells that passed
220 diagenesis screening (none of the excluded samples show significantly different $\delta^{18}O_{carb}$ values, only two exhibit lower-than-normal $\delta^{13}C_{carb}$, and one has a higher-than-normal Δ_{47}-derived temperature; Figs. S1, S2, S3). Additionally, the one sample of matrix material (taken from the Meerssen Member) showed a temperature of ~20 °C, indicating that the bulk matrix—

which is more likely to be affected by recrystallization or reordering than a dense calcite shell—has also not undergone isotopic alteration (Fig. S3).
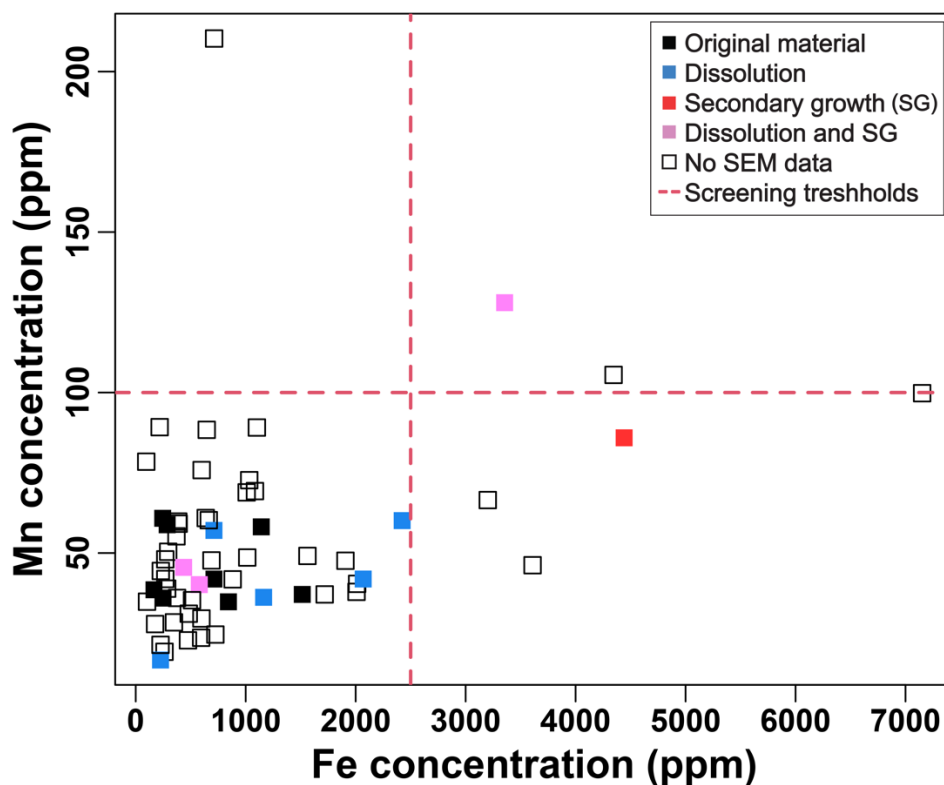
Figure 3: Iron and manganese concentrations of all samples, used for diagenesis screening. Dashed red lines represents screening thresholds of 2500 ppm for Fe and 100 ppm for Mn, selected to screen out most samples showing secondary growth while keeping most samples showing good preservation under SEM. This screening resulted in seven samples being excluded for elevated trace elements and two more for evidence of secondary growth under SEM (see text).

225

4.2 Stable isotopes

230

Of the 60 shell specimens measured for $\delta^{18}O_{carb}$ and $\delta^{13}C_{carb}$, nine were excluded from further interpretation due to evidence for diagenesis (described above). The remaining 51 specimens exhibit a range of $\delta^{18}O_{carb}$ values between -2.3 ‰ and -0.5 ‰ VPDB with the exception of two outliers that measured +0.4 ± 0.1 ‰ VPDB and +0.7 ± 0.1 ‰ VPDB (Fig. S1). Excluding these outliers, the average $\delta^{18}O_{carb}$ value throughout the section is -1.3 ± 0.4 ‰ VPDB. Although divergent samples in $\delta^{18}O_{carb}$ do not show divergent $\delta^{13}C_{carb}$ values, we nevertheless excluded them from further calculated averages. The resultant mean $\delta^{13}C_{carb}$ is 2.8 ± 0.6 ‰ VPDB with all values ranging between 1.4 ‰ and 4.0 ‰ VPDB (Fig. S2). The taxa *Neithea regularis, Rastellum* sp*., and Ceratostreon* sp. exhibit notably lower $\delta^{13}C$ values (1.6–2.2 ‰) relative to other species, potentially indicating higher incorporation of metabolic carbon, but $\delta^{18}O_{carb}$ values remain similar to other taxa. No other

235

taxa show distinguishable offsets from the mean $\delta^{18}O_{carb}$ or $\delta^{13}C_{carb}$ values (Figs. S1, S2). Nevertheless, the number of
240   specimens representing most of the taxa is too small to make reliable conclusions.

Bulk carbonate $\delta^{18}O$ analysis of the Maastricht Formation at ENCI quarry reveals an increasing then stabilizing trend from
the bottom of the formation toward the top (Vellekoop et al., in prep.) (Fig. S1). The lowest bulk carbonate $\delta^{18}O$ values (less
than -1.6 ‰ VPDB) occur in the Valkenberg Member where bulk carbonate values align with bivalve $\delta^{18}O_{carb}$ values (Fig.
245   S1). Above the Valkenberg Member, bulk matrix $\delta^{18}O_{carb}$ increases steadily through the Gronsveld and Schiepersberg
Members before leveling off between -0.55 ‰ and -0.03 ‰ VPDB throughout the Emaël and Nekum Members (Fig. S1).
Over this interval, bivalve $\delta^{18}O_{carb}$ values are generally lower than the bulk carbonate, with values ranging between -1.6 ‰
and -0.5 ‰ VPDB in the Emaël and Nekum Members (Fig. S1). This relationship holds true in the Meerssen member, where
the matrix sample measured as part of this study is elevated above bivalve $\delta^{18}O_{carb}$ by ~1 ‰ on average and continues the
250   constant trend in bulk carbonate $\delta^{18}O_{carb}$ from the Emaël and Nekum Members, plotting at -0.5 ‰ VPDB (Fig. S1).
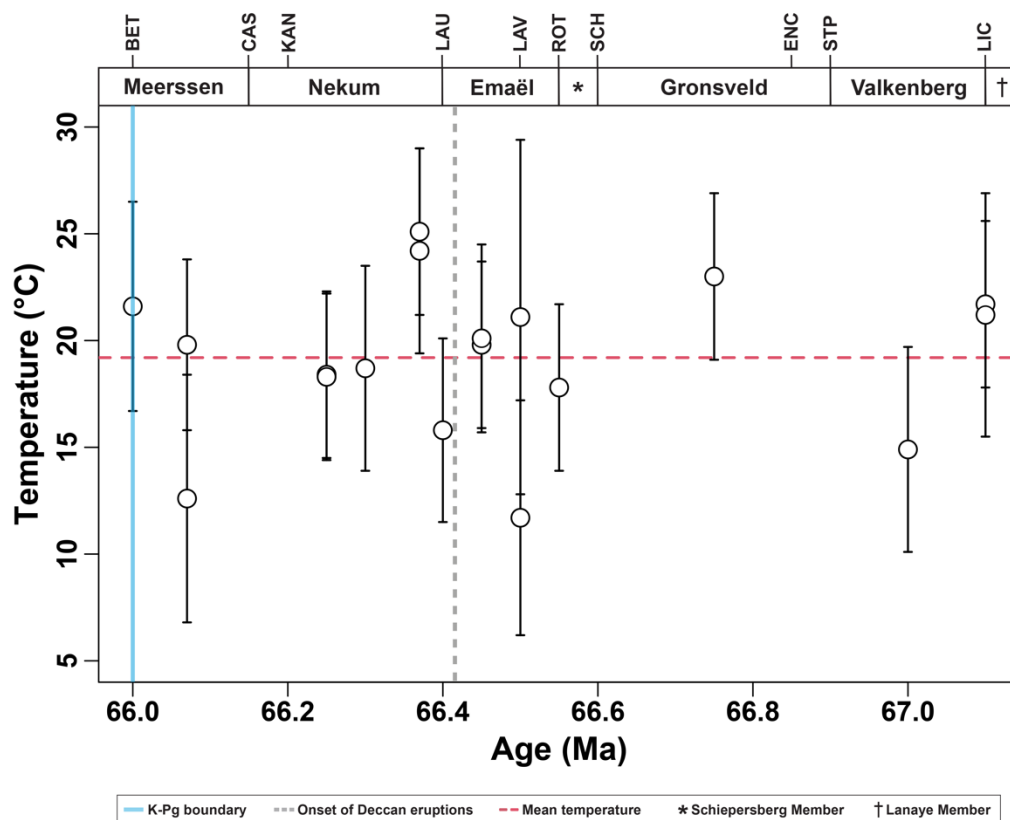
Figure 4: Maastrichtian paleotemperatures derived from Δ_{47}. Both internal and external standard error were calculated for all data
points, and the larger of the two errors for each point is depicted here as an error bar. Samples that did not pass SEM and trace element
diagenesis screening are not included on this plot. Onset of the main Deccan Traps eruptions (grey dotted line) at 66.413 Ma (Sprain et al.,
255   2019). K-Pg boundary (blue line) at 66.0 Ma. Mean temperature of 19.2 °C (red dashed line). Member names and horizon abbreviations
are labeled across top of figure.

4.3 Temperature estimates

Four of the 21 shell specimens measured for Δ_{47} were excluded from further interpretation as part of the group of nine
samples displaying evidence of diagenesis (described above) (Fig. S3). The 17 samples that pass diagenetic screening criteria
260 exhibit paleotemperatures ranging from 11.7–25.1 °C with a mean value of 19.2 ± 3.8 °C (Fig. 4). In the four instances
where multiple taxa were sampled from the same horizon, there is generally strong agreement between reconstructed
temperatures (all but one have means within 1 °C, well within error). A fluctuating temporal trend is observed in which
paleotemperatures peak at 66.37 Ma, followed by a decrease by 66.1 Ma. The sample from the shell hash layer representing
the KPB in the GSGs indicates a second warming from 66.1 to the boundary at 66.0 Ma of ~9 °C, though this trend relies on
265 only two datapoints (Fig. 4). The initial warming coincides with the named "Late Maastrichtian Warm Event" (Woelders et
al., 2018, Hull et al., 2020) and the onset of Deccan volcanism 66.413 ± 0.067 Ma (Sprain et al., 2019), within the error of
our age model.
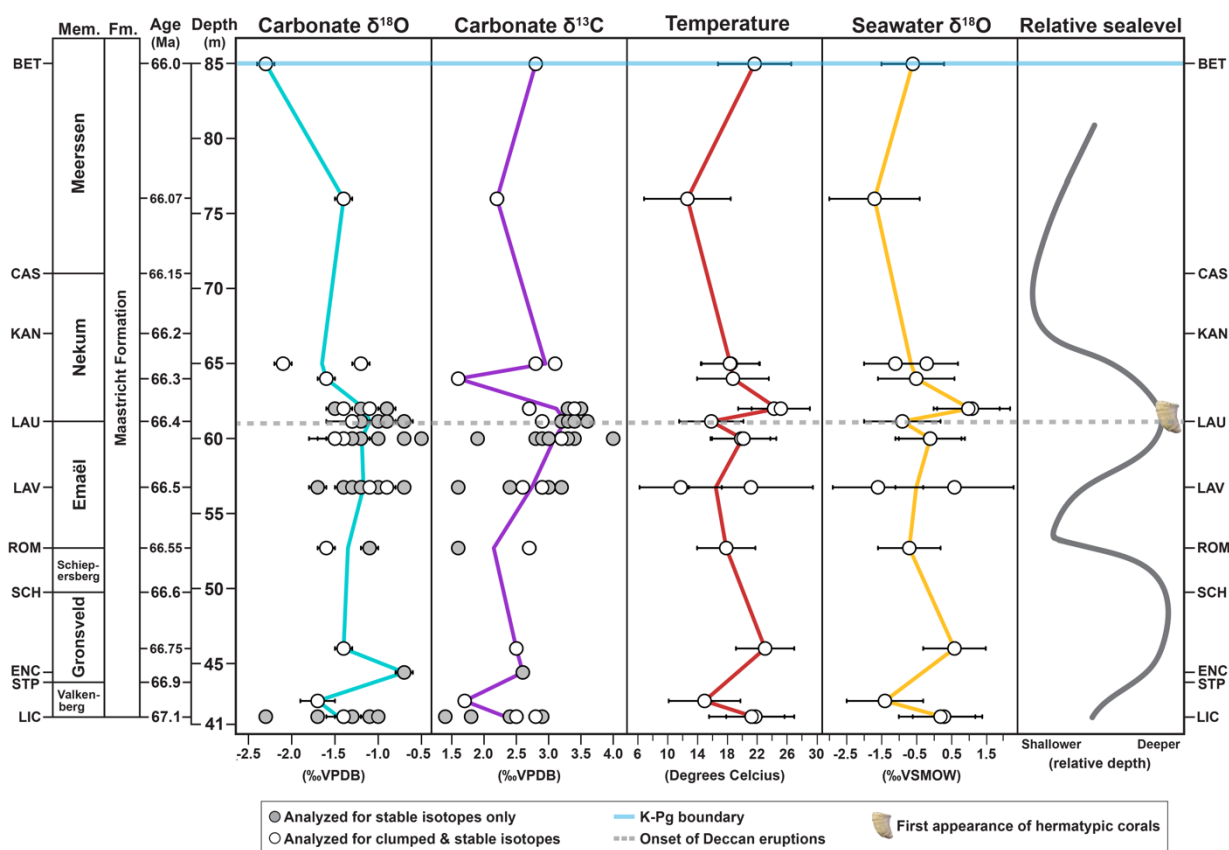
**Figure 5: Isotopic composition and paleotemperature measurements compared to inferred relative sea level in the Maastricht
270 Formation.** For horizons with more than one data point for one parameter, the average of all points in that horizon is intersected by the
trendline. If no error bars are visible, the uncertainty is smaller than the size of the symbol. Age model from Vellekoop et al. (in prep.).
The relative sea level curve is based on that derived by Schiøler et al. (1997) and fitted to the depth/age model used in this study.
Hermatypic coral appearance data is from Leloux (1999). Onset of the main Deccan Traps eruptions (grey dotted line) at 66.413 Ma
(Sprain et al., 2019). K-Pg boundary (blue line) at 66.0 Ma.

4.4 Seawater δ¹⁸O estimates

Calculated $\delta^{18}O_{sw}$ values ranged from -1.7 to 1.1 ‰ VSMOW (Fig. 5). The average $\delta^{18}O_{sw}$ value is -0.3 ± 0.9 ‰ VSMOW, above but within error of the ice-free mean ocean water estimate of -1.0 ‰ VSMOW. This heavier average $\delta^{18}O_{sw}$ value is consistent with the presence of some continental ice volume (presumed to be located on the Antarctic continent) during the "cool greenhouse" Maastrichtian interval (Miller et al., 2005; Petersen et al., 2016a, Ladant and Donnadieu, 2016). There are generally no significant offsets in $\delta^{18}O_{sw}$ between taxa when multiple taxa were sampled within a given horizon. These data show a similar temporal trend to that of the paleotemperature data (Fig. 5). The similarity in trajectories between temperature and $\delta^{18}O_{sw}$ is required because temperature shows no correlation with $\delta^{18}O_{carb}$ (Fig. 5).

We observe peak $\delta^{18}O_{sw}$ values at the base of the Nekum Member (1.1 ± 1.1 ‰ VSMOW; depth of ~62 m), while the lowest $\delta^{18}O_{sw}$ values occur at the Lava Horizon in the Emaël Member (one sample at -1.6 ± 1.3 ‰ VSMOW; depth of 56.75 m) and in the middle part of the Meerssen Member (-1.7 ± 1.3 ‰ VSMOW; depth of ~76 m) (Fig. 5). The $\delta^{18}O_{sw}$ values appear to fluctuate in time with similar variations in temperature and $\delta^{13}C_{carb}$ (Fig. 5).
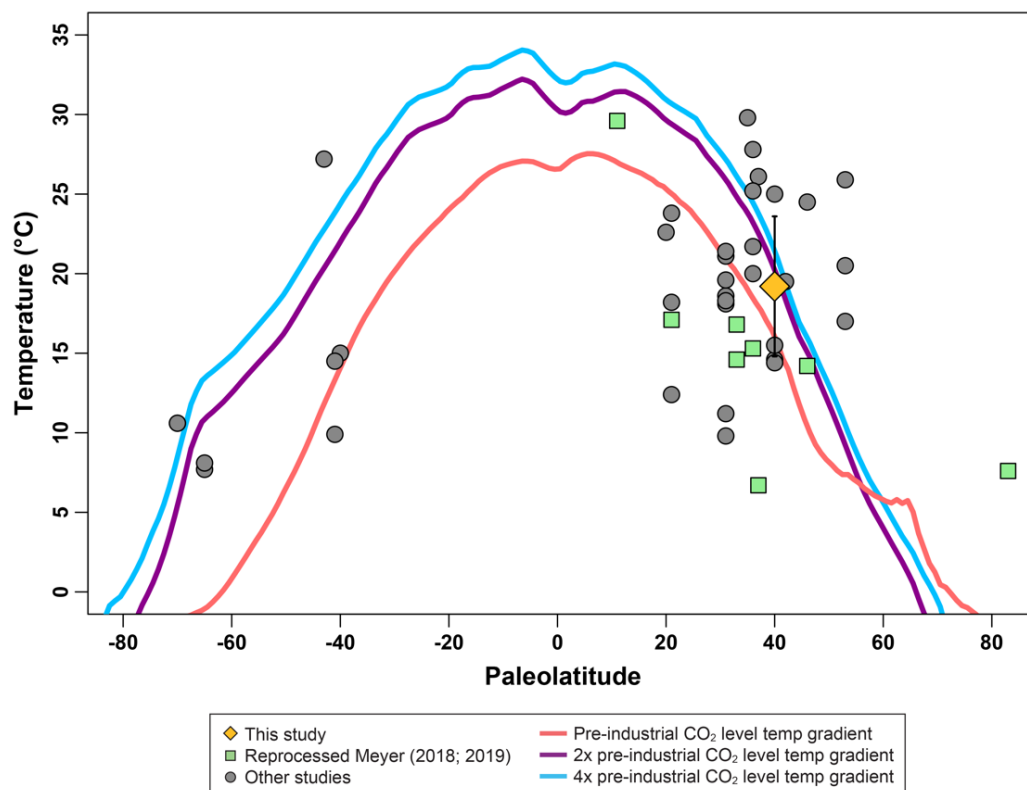
Figure 6: Average late Maastrichtian temperatures from numerous clumped isotope studies at different paleolatitudes around the globe. New data from this study and reprocessed data from Meyer et al. (2018; 2019) are included. The three lines are global climate models created with Late Cretaceous conditions and varying pCO₂ levels (Tabor et al., 2016). All studies used in this figure are listed in Table S1.

4.5 Revised temperature estimates from previously published clumped isotope data

Reprocessing of published Maastrichtian clumped isotope data from Meyer et al. (2018; 2019) resulted in substantially
295 higher (~6 °C) average temperatures for four locations and slightly lower (>1 °C) average temperatures for the remaining
four sites (Table 1). Our reprocessed Meyer et al. (2018; 2019) temperatures align more closely with previously published
data and modeling studies (Fig. 6). Notably, an originally anomalously low paleotemperature of 6.7 °C for a sample from the
Navesink Formation in Monmouth County, New Jersey (paleolatitude of 37° N; Meyer et al., 2018) increased to 13.8 °C
after reprocessing (Table 1).

300

Table 1: Clumped isotope-derived temperatures from Meyer et al. (2018; 2019) reprocessed using the same procedure as our data.
Data from this study is included and highlighted in red. Paleolatitudes determined via www.paleolatitude.org (van Hinsbergen et al.,
2015), apart from the Moreno Formation study by Meyer et al. (2019) for which paleolatitude was estimated by Kodama and Ward (2001)
due to the location being on an unconstrained plate.

305

Study	Sample type	Formation and locality	Paleolat. (°N)	Approx. age (Ma)	Original avg. temp. (°C)	Reprocessed avg. temp. (°C)
Meyer et al. (2018)	Oysters	Navesink Formation Monmouth County, NJ, USA	37	70.7	6.7	13.8
Meyer et al. (2018)	Oysters, clams, gastropod	Ripley Formation Western Tennessee, USA	36	73.5	15.3	21.5
Meyer et al. (2018)	Oysters, clams	Clayton, Prairie Bluff, Ripley Fms. Moscow Landing, AL, USA	33	65.0–74.0	16.8	22.1
Meyer et al. (2018)	Oysters, clams, belemnite	Pee Dee Formation Burches Ferry, SC, USA	33	71.4	14.6	20.6
Meyer et al. (2019)	Clam, bivalve	Prince Creek Formation North Slope, AK, USA	83	69.4	7.6	7.4
Meyer et al. (2019)	Belemnites, bivalve	Unidentified formation Scania, Sweden	46	69.2–72.3	14.2	13.9
Meyer et al. (2019)	Oysters, clams	Moreno Formation Merced County, CA, USA	21	69.7–78.0	17.1	16.5
Meyer et al. (2019)	Oysters	Unknown formation Fezzan region, Libya	11	70.9–71.4	29.6	29.2
This study	Oysters, clams, scallops	Maastricht Formation SE Netherlands & NE Belgium	40	66.0–66.8	NA	19.2

5 Results

5.1 Local to global Maastrichtian climate

New data presented here indicates mean annual ocean temperatures in the Maastricht region (paleolatitude ~40° N; van
310 Hinsbergen et al., 2015) varied from 11.7–25.1 °C between 67.1–66.0 Ma, with a mean temperature of 19.2 ± 3.8 °C. This is

much warmer than the modern-day climate of Maastricht but agrees closely with the mean of other published Maastrichtian marine paleotemperatures from sites located between 30–50° N (mean of 19.8 ± 5.2 °C; n = 23 studies; Table S1). For comparison, modern-day Maastricht has an average annual air temperature of 9.8 °C (Maastricht Climate, 2021). New paleotemperature estimates also align with evidence from Maastrichtian-aged fossil plants which suggest that on-land

315   temperatures at 40° N were around 15 °C (Golovneva, 2000) and that near 49° N, air temperatures varied from 10–18 °C during this time interval (Wilf et al., 2003). Our mean temperature also agrees well with zonal mean temperatures generated by general circulation models using Late Cretaceous paleogeography and atmospheric pCO$_2$ levels of either two- or four-times pre-industrial levels (Tabor et al., 2016; Ladant et al., 2020) (Fig. 6).

5.2 Ocean circulation, sea level, and/or precipitation changes

320   Paleogeographic reconstructions (Engelke et al., 2017; Scotese, 2021) (Fig. 1a) and presence of seagrass fossils (Hart et al., 2016; van der Ham et al., 2017) indicate that during the Campanian-Maastrichtian, the study site was located on a large, shallowly submerged carbonate platform. Over the Late Cretaceous, eustatic sea level fluctuated multiple times, including one sea level transgression (KMa5) in the latest Maastrichtian at 66.8 Ma (Haq, 2014). Sea level based on the relative abundance of the palynomorph *Paralecaniella* in ENCI quarry sediments—the same section as our fossils—indicate

325   Maastrichtian fluctuations that differ from the global eustatic curve (Schiøler et al., 1997) (Fig. 5). Since high relative abundances of this acritarch taxon are suggested to reflect marginal-marine to restricted-marine conditions under high hydrodynamic conditions (Brinkhuis and Schiøler 1996; Schiøler et al., 1997), observed fluctuations are interpreted as local sea level changes. Nevertheless, seagrass and foraminifera indicate that water depths remained less than 20 m at all times, and often shallower (Hart et al., 2016).

330

Although this local sea level record derived from palynological abundances may have some issues at a fine scale related to minimal consideration of sedimentology and geochemistry (Vellekoop et al., in prep.), we see a notable correlation between it and many of our isotopic parameters. Peak $\delta^{18}O_{sw}$ values, high temperatures, and higher $\delta^{13}C_{carb}$ values correlate to periods of maximum sea level, while lower $\delta^{18}O_{sw}$ values, cooler temperatures, and lower $\delta^{13}C_{carb}$ values correspond to periods of

335   relatively lower sea level (Fig. 5). Alternatively, environmental factors other than sea level might have driven the observed high abundances of *Paralecaniella* in the type-Maastrichtian, such as biological responses to local changes in hydrodynamic conditions and salinity, which would also be reflected in the $\delta^{18}O_{sw}$ record presented here.

We propose that the observed correlation between environmental conditions and reconstructed local sea level is the result of

340   fluctuating ocean circulation patterns. Paleogeographic reconstructions suggest the presence of a seaway connecting the Arctic Ocean to this study site during the Late Maastrichtian (Engelke et al., 2017; Scotese, 2021) (Fig. 1a). Modeling studies show that increased isolation of the Arctic made it fresher during the Maastrichtian (Ladant et al., 2020), suggesting that this boreal water mass was both cooler in temperature and depleted in $\delta^{18}O$. As a result, the Maastrichtian type region

would have been under the influence of relatively cool, depleted water masses. Our study site was situated on a shallow
carbonate platform surrounded by small landmasses, the exact size and position of which are difficult to define (Engelke et
al., 2017; Scotese, 2021) (Fig. 1a). During periods of low relative sea level, the land masses of the Rhenohercynian Zone
(Rhenish Massif, London-Brabant Massif) would have blocked southern currents originating in warmer regions, which
would likely be saltier and have higher $\delta^{18}O_{sw}$ values due to evaporative enrichment. However, as large parts of these land
masses were relatively flat and low-lying during the Upper Cretaceous (Vandenberghe et al., 2014), relatively minor
increases in sea level could potentially breach sills or island barriers, changing both the position of ocean currents and the
dominant water mass in a given area. Indeed, lithostratigraphic studies in the region have shown that during various phases
in the Campanian-Maastrichtian, the structural highs of the nearby London-Brabant Massif were fully submerged (e.g.,
Dusar and Lagrou, 2007). As a result, during sea level lows, the Maastrichtian type region would have been predominantly
under the influence of colder, depleted water masses, while during sea level highs, the influence of warmer, more enriched
water masses likely increased.

Similar interactions between cooler and warmer water masses have been called upon to explain unexpected distributions in
warm-water ammonite fauna in the Coniacian-Santonian of Europe (Remin et al., 2016) and remarkably southerly
occurrences of cold-water belemnites in Late Cenomanian France (Gale and Christensen, 1996). In this case, the authors
suggest that warm waters flowing east to west from the proto-Tethys competed with cooler waters flowing southward
between Greenland and Scandinavia (see their Figure 10). We suggest a similar mechanism applied to Late Maastrichtian
paleogeography and water masses (Fig. 1a). Ostracod assemblage changes indicate increasing contribution of warm
Mediterranean/Tethyan waters in the latest Maastrichtian (Bless, 1988). Faunal abundance differences along the US East
Coast indicate the presence of an ancient Gulf Stream-like current as far back in time as the Maastrichtian (Watkins and Self-
Trail, 2005), which would have warmed the Maastricht region above its expected temperature for latitude when bathed in
water from the south, as the modern-day Gulf Stream does for western Europe. In summary, the cooler water mass may have
originated in the Arctic, whereas the warmer water mass may have come from the southwest (Fig. 1a).

Fluctuations in $\delta^{13}C$ appear to correlate with changes in temperature and $\delta^{18}O_{sw}$ (Fig. 5). In this hypothetical model of
alternating influence of southern and northern source waters, this could indicate different $\delta^{13}C$ of dissolved inorganic carbon
($\delta^{13}C_{DIC}$) in the two water masses. The exact values of $\delta^{13}C_{DIC}$ in either water mass are difficult to define because of
overprinting by $\delta^{13}C$ vital effects in some taxa (*Neithia* sp*., Rastellum* sp.). Looking at the most common taxa (*Acutostrea*),
variations on the order of 0.5‰ VPDB—or possibly as much as 1 ‰—are possible between horizons. This is similar to
variability seen in the modern Atlantic Ocean (Eide et al., 2017) and is therefore plausibly driven by alternating water
masses of differing $\delta^{13}C_{DIC}$. In this scenario, the colder, northern (Arctic) water mass would be more depleted in $\delta^{13}C_{DIC}$ than
the southern source water.

This dataset is not capable of distinguishing between the above, preferred hypothesis and a temporally variable input of isotopically depleted freshwater. During times of lower sea level, partial basin restriction may have occurred, allowing local

380   freshwater inputs to lower $\delta^{18}O_{sw}$ values. In maritime regions such as modern Bermuda, despite lack of elevation or substantial landmass, precipitation is depleted in $\delta^{18}O$ by 4–5 ‰ VSMOW relative to seawater (Zhang et al., 2021). Additionally, surface runoff may contain dissolved terrestrial organic matter depleted in $\delta^{13}C$, which could explain the correlation between $\delta^{18}O_{sw}$ and $\delta^{13}C$ through our study period. However, it is difficult to explain how local freshwater in a subtropical environment surrounded by low-lying landmasses could be substantially colder than local seawater, so we favor

385   the variable water mass hypothesis over a local freshwater contribution.

Yet another possible interpretation of the co-variation between fluctuating temperature and $\delta^{18}O_{sw}$ trends is via climate-related reorganization of atmospheric circulation, moving broad precipitation bands north and south over the study region. An enhanced hydrological cycle has been hypothesized for the latest Cretaceous (e.g., Woelders et al., 2017) due to

390   increased zonal surface winds and ~20 % stronger Hadley circulation in the Northern Hemisphere (Bush and Philander, 1997). If, during warmer climates, precipitation bands moved such that the Maastrichtian type region experienced less rainfall, $\delta^{18}O$ enrichment of surface waters would coincide with warmer temperatures and vice versa. This is difficult to assess, even in global climate model simulations, as model proficiency in reconstructing paleo-precipitation regimes is difficult to validate/calibrate. The rough correlation with $\delta^{13}C$ is also difficult to explain in this scenario.

395   **5.3 Temperature trends and a record of Deccan-induced warming**

Multiple paleoclimate records document a late Maastrichtian warming event (LMWE) (e.g., Stott and Kennett, 1990; Li and Keller, 1998; Petersen et al., 2016a; Woelders et al., 2017; Woelders et al., 2018; Barnet et al., 2019; Gao et al., 2021; Nava et al., 2021), beginning gradually at 66.4 Ma with more rapid warming at 66.3 Ma (Hull et al., 2020). This timing of the LMWE aligns it with the onset of LIP volcanism in the Indian subcontinent, based on [40]Ar-[39]Ar ages for the oldest basalts of

400   the Deccan Traps (66.413 ± 0.067 Ma; Sprain et al., 2019) and shifts in marine osmium isotope ratios towards mantle values beginning ~400 kyr prior to the KPB (Ravizza and Peucker-Ehrenbrink, 2003; Hull et al., 2020).

The Δ_{47}-derived temperature record generated here documents a warming in the Nekum Member from 66.4 Ma (15.8 ± 4.3 °C) to 66.37 Ma (24.7 ± 4.8 °C) (Fig. 4). The magnitude of this warming is calculated as 8.9 °C going from adjacent

405   horizons or, more conservatively, 7.0 °C comparing the warmest horizon to a pre-event baseline averaging the preceding six points (17.7 ± 3.5 °C). Considering the size and meaning of the 1SE error bars and the small number of samples representing peak warmth (n=2; Fig. 4), this warming event is only barely distinguishable as differing from the mean of the full record. However, a number of other lines of evidence support the interpretation of this warming as an expression of the LMWE.

410 Based on a newly updated age model (Vellekoop et al., in prep), the warmest Δ_{47}-derived temperatures align with the onset of earliest Deccan eruptions and the age of the globally defined LMWE (Fig. 4). The dinocyst *Palynodinium grallator*—a marker for the LMWE at northern mid-latitudes (Vellekoop et al., 2018; 2019)—first appears in the Maastricht Formation in the Nekum Member (Schioler et al., 1997; Vellekoop et al., 2019). Thermophilic hermatypic scleratinian macrofossils also first emerge in high abundances in the Nekum Member (Liebau, 1978; Leloux, 1999). Together, these records suggest that
415 the LMWE is preserved in the Nekum Member at ENCI quarry and that the warmer Δ_{47}-derived temperatures found there are likely real.

We observe a second warming directly preceding the boundary (~66.1 Ma) in our record (Fig. 4), which is also visible in other records (e.g., Wilf et al., 2003; Petersen et al., 2016a, Woelders et al., 2017; Zhang et al., 2018). The magnitude of this
420 second warming is uncertain given the low density of samples immediately prior from which to determine a baseline pre-excursion temperature, and suffers from the same statistical issues as defining the LMWE (limited samples, large 1SE error bars). Therefore, we opt not to overinterpret this. A higher sample density through this section could potentially resolve some of this uncertainty.

6 Conclusions

425 This study presents a new clumped isotope-based paleotemperature time series from the latest Cretaceous in northwestern Europe. The Δ_{47} analyses from the Maastrichtian type section and surrounding outcrops reveal a mean temperature of 19.2 ± 3.8 °C and an average $\delta^{18}O_{sw}$ of -0.3 ± 0.9 ‰ VSMOW, consistent with a subtropical shallow marine environment. This average temperature aligns well with other paleothermometry studies from similar paleolatitudes and with modeled Maastrichtian paleotemperatures. Increasing Δ_{47}-based temperatures at ~66.4 Ma, in conjunction with other indicators, are
430 interpreted to reflect a regional manifestation of the global LMWE and directly link pre-KPB warming in northwest Europe to CO_2 emissions from Deccan Traps volcanism.

Covariations in temperature, $\delta^{18}O_{sw}$, and (to a lesser degree) $\delta^{13}C$ from horizon to horizon may reflect the varying influences of different water mass at different times. We hypothesize that colder waters with lower $\delta^{18}O_{sw}$ and $\delta^{13}C_{DIC}$ may have
435 originated from the Arctic and reached the study site via a passageway between Greenland and Scandinavia (Fig. 1a). Warmer waters with higher $\delta^{18}O_{sw}$ and $\delta^{13}C_{DIC}$ may have been sourced from a proto-Tethys to the southeast or proto-Atlantic to the southwest (Fig. 1a). Alternating influence of these two proposed water masses may be linked to regionally fluctuating sea level and the presence of more submerged or more exposed bathymetric highs allowing or preventing southern water flowing north.

440

Overall, the fossils of the Maastricht Formation are effective paleotemperature archives that reveal linkages between local sea level changes, Deccan Traps volcanism, and ocean temperature on the European continent in the lead-up to the end-Cretaceous.

Data availability

445 All data presented in this paper are available in the EarthChem database at https://doi.org/10.26022/IEDA/112046.

Further data are available in the Supplement:

- Figure S1: oxygen isotope values of shell specimens and bulk carbonate;
- Figure S2: carbon isotope values of shell specimens and bulk carbonate;
- Figure S3: all Δ_{47}-derived paleotemperature data, including samples removed due to diagenesis;
450 - Table S1: average paleotemperature data for all Maastrichtian-aged studies reconstructing marine temperatures used to create Figure 6;
- Table S2: all data for all samples including SEM results, trace elements, stable and clumped isotopes, paleotemperatures, and $\delta^{18}O$ of seawater.

Author contribution

455 HEO, SVP, and JV designed the study. SVP and JV collected the samples. HEO, SVP, MMJ, and SRS measured and analysed the data. HEO prepared the manuscript, with contributions from all co-authors.

Competing interests

The authors declare that they have no conflicts of interest.

Acknowledgements

460 We are grateful to Ashling Neary (SCIPP lab) and Angela Dial (MEAL) for assisting in sample preparation and measurements at the University of Michigan. We would also like to thank the Department of Earth and Environmental Sciences for the Graduate Turner Award and the Geologic Society of America for the Graduate Student Research Grant, both of which helped to fund this project.

References

465 Barnet, J. S. K., Littler, K., Westerhold, T., Kroon, D., Leng, M. J., Bailey, I., Röhl, U., and Zachos, J. C.: A High-fidelity benthic stable isotope record of Late Cretaceous–Early Eocene climate change and carbon-cycling, Paleoceanogr. Paleoclimatol., 34, 672–691, https://doi.org/10.1029/2019PA003556, 2019.

Bernasconi, S. M., Daëron, M., Bergmann, K. D., Bonifacie, M., Meckler, A. N., Affek, H. P., et al.: InterCarb: A
470 community effort to improve interlaboratory standardization of the carbonate clumped isotope thermometer using carbonate standards. Geochem., Geophy., Geosy., 22, https://doi.org/10.1029/2020GC009588, 2021.

Bless, M. J. M.: Possible causes for the change in ostracod assemblages at the Maastrichtian-Palaeocene boundary in southern Limburg, The Netherlands, Meded. Werkgr. Tert. Kwart. Geol., 25, 197–211, 1988.

475

Bowman, V. C., Riding, J. B., Francis, J. E., Crame, J. A., and Hannah, M. J.: The taxonomy and palaeobiogeography of small chorate dinoflagellate cysts from the Late Cretaceous to Quaternary of Antarctica, Palynology, 37, 151–169, https://doi.org/10.1080/01916122.2012.750898, 2013.

480 Brand, U. and Morrison, J. O.: Biogeochemistry of fossil marine invertebrates. Geosci. Can., 14, 1987.

Brinkhuis, H. and Schiøler, P.: Palynology of the Geulhemmerberg Cretaceous/Tertiary boundary section (Limburg, SE Netherlands), Geol. Mijnbouw, 75, 193–213, 1996.

485 Bush, A. B. G. and Philander, S. G. H.: The Late Cretaceous: Simulation with a coupled atmosphere-ocean general circulation model, Paleoceanography, 12, 495–516, https://doi.org/10.1029/97PA00721, 1997.

Came, R. E., Brand, U., and Affek, H. P.: Clumped isotope signatures in modern brachiopod carbonate, Chem. Geol., 377, 20–30, https://doi.org/10.1016/j.chemgeo.2014.04.004, 2014.

490

Clyde, W. C., Ramezani, J., Johnson, K. R., Bowring, S. A., and Jones, M. M.: Direct high-precision U–Pb geochronology of the end-Cretaceous extinction and calibration of Paleocene astronomical timescales, Earth Planet. Sci. Lett., 452, 272–280, https://doi.org/10.1016/j.epsl.2016.07.041, 2016.

495   de Winter, N. J. D., Vellekoop, J., Vorsselmans, R., Golreihan, A., Soete, J., Petersen, S. V., Meyer, K. W., Casadio, S., Speijer, R. P., Claeys, P.: An assessment of latest Cretaceous Pycnodonte vesicularis (Lamarck, 1806) shells as records for palaeoseasonality: a multi-proxy investigation, Clim. Past, 14, 725–749, https://doi.org/10.5194/cp-14-725-2018, 2018.

Defliese, W. F., Hren, M. T., and Lohmann, K. C.: Compositional and temperature effects of phosphoric acid fractionation
500   on Δ_{47} analysis and implications for discrepant calibrations, Chem. Geol., 396, 51–60, https://doi.org/10.1016/j.chemgeo.2014.12.018, 2015.

Dennis, K. J., Affek, H. P., Passey, B. H., Schrag, D. P., and Eiler, J. M.: Defining an absolute reference frame for 'clumped' isotope studies of CO_2, Geochim. Cosmochim. Ac., 75, 7117–7131, https://doi.org/10.1016/j.gca.2011.09.025, 2011.

505

Dennis, K. J., Cochran, J. K., Landman, N. H., and Schrag, D. P.: The climate of the Late Cretaceous: New insights from the application of the carbonate clumped isotope thermometer to Western Interior Seaway macrofossil, Earth Planet. Sci. Lett., 362, 51–65, https://doi.org/10.1016/j.epsl.2012.11.036, 2013.

510   Dortangs, R. W., Schulp, A. S., Mulder, E. W., Jagt, J. W., Peeters, H. H., and De Graaf, D. T.: A large new mosasaur from the Upper Cretaceous of The Netherlands, Neth. J. Geosci., 81, 1–8, https://doi.org/10.1017/S0016774600020515, 2002.

Dusar, M. and Lagrou, D.: Cretaceous flooding of the Brabant Massif and the lithostratigraphic characteristics of its chalk cover in northern Belgium, Geol. Belg., 10, 27–38, 2007.

515

Eagle, R. A., Eiler, J. M., Tripati, A. K., Ries, J. B., Freitas, P. S., Hiebenthal, C., Wanamaker Jr, A. D., Taviani, M., Elliot, M., and Marenssi, S.: The influence of temperature and seawater carbonate saturation state on ^{13}C–^{18}O bond ordering in bivalve mollusks, Biogeosciences, 10, 4591–4606, https://doi.org/10.5194/bg-10-4591-2013, 2013.

520   Eide, M., Olsen, A., Ninnemann, U. S., and Johannessen, T.: A global ocean climatology of preindustrial and modern ocean $\delta^{13}C$, Global Biogeochem. Cy., 31, 515–534, https://doi.org/10.1002/2016GB005472, 2017.

Eiler, J. M.: Paleoclimate reconstruction using carbonate clumped isotope thermometry, Quaternary Sci. Rev., 30, 3575–3588, https://doi.org/10.1016/j.quascirev.2011.09.001, 2011.

525

Engelke, J., Linnert, C., Mutterlose, J., and Wilmsen, M.: Early Maastrichtian benthos of the chalk at Kronsmoor, northern Germany: implications for Late Cretaceous environmental change, Palaeobio. Palaeoenv., 97, 703–722, https://doi.org/10.1007/s12549-017-0283-2, 2017.

530 Felder, W. M.: Lithostratigrafie van het Boven-Krijt en het Dano-Montien in Zuid-Limburg en het aangrenzende gebied, Rijks Geologische Dienst (Haarlem), 63–72, 1975.

Fendley, I. M., Mittal, T., Sprain, C. J., Marvin-DiPasquale, M., Tobin, T. S., and Renne, P. R.: Constraints on the volume and rate of Deccan Traps flood basalt eruptions using a combination of high-resolution terrestrial mercury records and
535 geochemical box models, Earth Planet. Sci. Lett., 524, https://doi.org/10.1016/j.epsl.2019.115721, 2019.

Font, E., Adatte, T., Sial, A. N., de Lacerda, L. D., Keller, G., and Punekar, J.: Mercury anomaly, Deccan volcanism, and the end-Cretaceous mass extinction, Geology, 44, 171–174, https://doi.org/10.1130/G37451.1, 2016.

540 Gale, A. S. and Christensen, W. K.: Occurrence of the belemnite Actinocamax plenus in the, B. Geol. Soc. Denmark, 43, 68–77, 1996.

Gao, Y., Ibarra, D. E., Rugenstein, J. K. C., Chen, J., Kukla, T., Methner, K., Gao, Y., Huang, H., Lin, Z., and Zhang, L.: Terrestrial climate in mid-latitude East Asia from the latest Cretaceous to the earliest Paleogene: A multiproxy record from
545 the Songliao Basin in northeastern China, Earth-Sci. Rev., 216, https://doi.org/10.1016/j.earscirev.2021.103572, 2021.

Golovneva, L. B.: The Maastrichtian (Late Cretaceous) climate in the northern hemisphere, Geol. Soc. London Spec. Publ., 181, 43–54, https://doi.org/10.1144/GSL.SP.2000.181.01.05, 2000.

550 Haq, B. U.: Cretaceous eustasy revisited, Global Planet. Change, 113, 44–58, https://doi.org/10.1016/j.gloplacha.2013.12.007, 2014.

Hart, M. B., FitzPatrick, M. E., and Smart, C. W.: The Cretaceous/Paleogene boundary: Foraminifera, sea grasses, sea level change and sequence stratigraphy, Palaeogeogr. Palaeocl., 441, 420–429, https://doi.org/10.1016/j.palaeo.2015.06.046, 2016.
555
Henkes, G. A., Passey, B. H., Wanamaker Jr, A. D., Grossman, E. L., Ambrose Jr, W. G., and Carroll, M. L.: Carbonate clumped isotope compositions of modern marine mollusk and brachiopod shells, Geochim. Cosmochim. Ac., 106, 307–325, https://doi.org/10.1016/j.gca.2012.12.020, 2013.

560 Henkes, G. A., Passey, B. H., Grossman, E. L., Shenton, B. J., Pérez-Huerta, A., and Yancey, T. E.: Temperature limits for preservation of primary calcite clumped isotope paleotemperatures, Geochim. Cosmochim, Ac., 139, 362–382, https://doi.org/10.1016/j.gca.2014.04.040, 2014.

Hull, P. M., Bornemann, A., Penman, D. E., Henehan, M. J., Norris, R. D., Wilson, P. A., Blum, P., Alegret, L., Batenburg, S. J., and Bown, P. R.: On impact and volcanism across the Cretaceous-Paleogene boundary, Science, 367, 266–272, https://doi.org/10.1126/science.aay5055, 2020.

Jagt, J. W. M. and Jagt-Yazykova, E. A.: Stratigraphy of the type Maastrichtian–a synthesis, Scripta Geologica Special Issue, 8, 5–32, 2012.

Jagt, J. W., Donovan, S. K., Fraaije, R., Mulder, E. W., Nieuwenhuis, E., Stroucken, J., van Bakel, B., and van Knippenberg, P.: Remarkable preservation of selected latest Cretaceous macrofossils from the Maastrichtian type area (the Netherlands, Belgium), Fossil Record 4: Bulletin, 67, 75, 2016.

Keutgen, N.: A bioclast-based astronomical timescale for the Maastrichtian in the type area (southeast Netherlands, northeast Belgium) and stratigraphic implications: the legacy of PJ Felder, Neth. J. Geosci., 97, 229–260, https://doi.org/10.1017/njg.2018.15, 2018.

Kim, S. T. and O'Neil, J. R.: Equilibrium and nonequilibrium oxygen isotope effects in synthetic carbonates, Geochim. Cosmochim. Ac., 61, 3461–3475, https://doi.org/10.1016/S0016-7037(97)00169-5, 1997.

Kodama, K. P. and Ward, P. D.: Compaction-corrected paleomagnetic paleolatitudes for Late Cretaceous rudists along the Cretaceous California margin: Evidence for less than 1500 km of post–Late Cretaceous offset for Baja British Columbia, Geol. Soc. Am. Bull., 113, 1171–1178, https://doi.org/10.1130/0016-7606(2001)113%3C1171:CCPPFL%3E2.0.CO;2, 2001.

Ladant, J. B. and Donnadieu, Y.: Palaeogeographic regulation of glacial events during the Cretaceous supergreenhouse, Nat. Commun., 7, 1–9, https://doi.org/10.1038/ncomms12771, 2016.

Ladant, J. B., Poulsen, C. J., Fluteau, F., Tabor, C. R., MacLeod, K. G., Martin, E. E., Haynes, S. J., and Rostami, M. A.: Paleogeographic controls on the evolution of Late Cretaceous ocean circulation, Clim. Past, 16, 973–1006, https://doi.org/10.5194/cp-16-973-2020, 2020.

Land, L. S.: Diagenesis of skeletal carbonates, J. Sediment Res., 37, 914–930, https://doi.org/10.1306/74D717D5-2B21-11D7-8648000102C1865D, 1967.

Leloux, J.: Numerical distribution of Santonian to Danian corals (Scleractinia, Octocorallia) of southern Limburg, the Netherlands, Geol. Mijnbouw, 78, 191–195, https://doi.org/10.1023/A:1003743301625, 1999.

Li, L. and Keller, G.: Abrupt deep-sea warming at the end of the Cretaceous, Geology, 26, 995–998,
600 https://doi.org/10.1130/0091-7613(1998)026%3C0995:ADSWAT%3E2.3.CO;2, 1998.

Liebau, A.: Paläobathymetrische und paläoklimatische Veränderungen im Mikrofaunenbild der Maastrichter Tuffkreide, Neues Jahrb. Geol. P. A., 157, 233–237, 1978.

605 Luijendijk, E., Van Balen, R. T., Ter Voorde, M., and Andriessen, P. A. M.: Reconstructing the Late Cretaceous inversion of the Roer Valley Graben (southern Netherlands) using a new model that integrates burial and provenance history with fission track thermochronology, J. Geophys. Res.-Sol. Ea., 116, https://doi.org/10.1029/2010JB008071, 2011.

Maastricht Climate: https://en.climate-data.org/europe/the-netherlands/limburg/maastricht-893/#temperature-graph, last
610 access: 14 June 2021.

Meyer, K. W., Petersen, S. V., Lohmann, K. C., and Winkelstern, I. Z.: Climate of the Late Cretaceous North American Gulf and Atlantic Coasts, Cretaceous Res., 89, 160–173, https://doi.org/10.1016/j.cretres.2018.03.017, 2018.

615 Meyer, K. W., Petersen, S. V., Lohmann, K. C., Blum, J. D., Washburn, S. J., Johnson, M. W., Gleason, J. D., Kurz, A. Y., and Winkelstern, I. Z.: Biogenic carbonate mercury and marine temperature records reveal global influence of Late Cretaceous Deccan Traps, Nat. Commun., 10, 1–8, https://doi.org/10.1038/s41467-019-13366-0, 2019.

Miller, K. G., Wright, J. D., and Browning, J. V.: Visions of ice sheets in a greenhouse world, Mar. Geol., 217, 215–231,
620 https://doi.org/10.1016/j.margeo.2005.02.007, 2005.

Molina, E., Alegret, L., Arenillas, I., Arz, J. A., Gallala, N., Hardenbol, J., Salis, K. von, Steurbaut, E., Vandenberghe, N., and Zaghbib-Turki, D.: The global boundary stratotype section and point for the base of the Danian stage (Paleocene, Paleogene," Tertiary", Cenozoic) at El Kef, Tunisia-original definition and revision, Episodes, 29, 263–273, 2006.
625
Möller, P. and Kubanek, F.: Role of magnesium in nucleation processes of calcite, aragonite and dolomite, Neues Jb. Miner. Abh., 126, 199–220, 1976.

Nava, A. H., Black, B. A., Gibson, S. A., Bodnar, R. J., Renne, P. R., and Vanderkluysen, L.: Reconciling early Deccan
630   Traps CO_2 outgassing and pre-KPB global climate, P. Natl. Acad. Sci. USA, 118, https://doi.org/10.1073/pnas.2007797118,
2021.

Percival, L. M., Jenkyns, H. C., Mather, T. A., Dickson, A. J., Batenburg, S. J., Ruhl, M., Hesselbo, S. P., Barclay, R., Jarvis,
I., and Robinson, S. A.: Does large igneous province volcanism always perturb the mercury cycle? Comparing the records of
635   Oceanic Anoxic Event 2 and the end-Cretaceous to other Mesozoic events, Am. J. Sci., 318, 799–860,
https://doi.org/10.2475/08.2018.01, 2018.

Petersen, S. V., Dutton, A., and Lohmann, K. C.: End-Cretaceous extinction in Antarctica linked to both Deccan volcanism
and meteorite impact via climate change, Nat. Commun., 7, 1–9, https://doi.org/10.1038/ncomms12079, 2016a.

640

Petersen, S. V., Tabor, C. R., Lohmann, K. C., Poulsen, C. J., Meyer, K. W., Carpenter, S. J., Erickson, J. M., Matsunaga, K.
K., Smith, S. Y., and Sheldon, N. D.: Temperature and salinity of the Late Cretaceous western interior seaway, Geology, 44,
903–906, https://doi.org/10.1130/G38311.1, 2016b.

645   Petersen, S. V., Winkelstern, I. Z., Lohmann, K. C., and Meyer, K. W.: The effects of Porapak™ trap temperature on $\delta^{18}O$,
$\delta^{13}C$, and Δ_{47} values in preparing samples for clumped isotope analysis, Rapid Commun. Mass Sp., 30, 199–208,
https://doi.org/10.1002/rcm.7438, 2016c.

Petersen, S. V., Defliese, W. F., Saenger, C., Daëron, M., Huntington, K. W., John, C. M., Kelson, J. R., Bernasconi, S. M.,
650   Colman, A. S., and Kluge, T.: Effects of improved [17]O correction on interlaboratory agreement in clumped isotope
calibrations, estimates of mineral-specific offsets, and temperature dependence of acid digestion fractionation, Geochem.,
Geophy., Geosy., 20, 3495–3519, https://doi.org/10.1029/2018GC008127, 2019.

Pucéat, E., Lécuyer, C., Donnadieu, Y., Naveau, P., Cappetta, H., Ramstein, G., Huber, B. T., and Kriwet, J.: Fish tooth $\delta^{18}O$
655   revising Late Cretaceous meridional upper ocean water temperature gradients, Geology, 35, 107–110,
https://doi.org/10.1130/G23103A.1, 2007.

Ravizza, G. and Peucker-Ehrenbrink, B.: Chemostratigraphic evidence of Deccan volcanism from the marine osmium
isotope record, Science, 302, 1392–1395, https://doi.org/10.1126/science.1089209, 2003.

660

Remin, Z., Gruszczyński, M., and Marshall, J. D.: Changes in paleo-circulation and the distribution of ammonite faunas at the Coniacian–Santonian transition in central Poland and western Ukraine, Acta Geol. Pol., 66, https://doi.org/10.1515/agp-2016-0006, 2016.

665   Schiøler, P., Brinkhuis, H., Roncaglia, L., and Wilson, G. J.: Dinoflagellate biostratigraphy and sequence stratigraphy of the type Maastrichtian (Upper Cretaceous), ENCI Quarry, The Netherlands, Mar. Micropaleontol., 31, 65–95, https://doi.org/10.1016/S0377-8398(96)00058-8, 1997.

Schulte, P., Alegret, L., Arenillas, I., Arz, J. A., Barton, P. J., Bown, P. R., Bralower, T. J., Christeson, G. L., Claeys, P., and 670   Cockell, C. S.: The Chicxulub asteroid impact and mass extinction at the Cretaceous-Paleogene boundary, Science, 327, 1214–1218, https://doi.org/10.1126/science.1177265, 2010.

Scotese, C. R.: An Atlas of Phanerozoic Paleogeographic Maps: The Seas Come In and the Seas Go Out, Annu. Rev. Earth Pl. Sc., 49, 669–718, https://doi.org/10.1146/annurev-earth-081320-064052, 2021.
675
Sial, A. N., Chen, J., Lacerda, L. D., Frei, R., Tewari, V. C., Pandit, M. K., Gaucher, C., Ferreira, V. P., Cirilli, S., and Peralta, S.: Mercury enrichment and Hg isotopes in Cretaceous–Paleogene boundary successions: Links to volcanism and palaeoenvironmental impacts, Cretaceous Res., 66, 60–81, https://doi.org/10.1016/j.cretres.2016.05.006, 2016.

680   Smit, J.: The global stratigraphy of the Cretaceous-Tertiary boundary impact ejecta, Annu. Rev. Earth Pl. Sc., 27, 75–113, https://doi.org/10.1146/annurev.earth.27.1.75, 1999.

Smit, J. and Brinkhuis, H.: The Geulhemmerberg Cretaceous/Tertiary boundary section (Maastrichtian type area, SE Netherlands); summary of results and a scenario of events. Geol. Mijnbouw, 75, 283–293, 1996.
685
Sprain, C. J., Renne, P. R., Clemens, W. A., and Wilson, G. P.: Calibration of chron C29r: New high-precision geochronologic and paleomagnetic constraints from the Hell Creek region, Montana, Geol. Soc. Am. Bull., 130, 1615–1644, https://doi.org/10.1130/B31890.1, 2018.

690   Sprain, C. J., Renne, P. R., Vanderkluysen, L., Pande, K., Self, S., and Mittal, T.: The eruptive tempo of Deccan volcanism in relation to the Cretaceous-Paleogene boundary, Science, 363, 866–870, https://doi.org/10.1126/science.aav1446, 2019.

Stott, L. D. and Kennett, J. P.: The paleoceanographic and paleoclimatic signature of the Cretaceous/Paleogene boundary in the Antarctic: stable isotopic results from ODP Leg 113, in: Proceedings of the Ocean Drilling Program, Scientific Results,
695   113, 829–848, 1990.

Tabor, C. R., Poulsen, C. J., Lunt, D. J., Rosenbloom, N. A., Otto-Bliesner, B. L., Markwick, P. J., Brady, E. C., Farnsworth, A., and Feng, R.: The cause of Late Cretaceous cooling: A multimodel-proxy comparison, Geology, 44, 963–966, https://doi.org/10.1130/G38363.1, 2016.

700

Tagliavento, M., John, C. M., and Stemmerik, L.: Tropical temperature in the Maastrichtian Danish Basin: Data from coccolith Δ_{47} and δ^{18}O, Geology, 47, 1074–1078, https://doi.org/10.1130/G46671.1, 2019.

Tobin, T. S., Ward, P. D., Steig, E. J., Olivero, E. B., Hilburn, I. A., Mitchell, R. N., Diamond, M. R., Raub, T. D., and
705   Kirschvink, J. L.: Extinction patterns, δ^{18}O trends, and magnetostratigraphy from a southern high-latitude Cretaceous– Paleogene section: Links with Deccan volcanism, Palaeogeogr. Palaeocl., 350, 180–188, https://doi.org/10.1016/j.palaeo.2012.06.029, 2012.

Tobin, T. S., Wilson, G. P., Eiler, J. M., and Hartman, J. H.: Environmental change across a terrestrial Cretaceous-Paleogene
710   boundary section in eastern Montana, USA, constrained by carbonate clumped isotope paleothermometry, Geology, 42, 351– 354, https://doi.org/10.1130/G35262.1, 2014.

Tobin, T. S., Bitz, C. M., and Archer, D.: Modeling climatic effects of carbon dioxide emissions from Deccan Traps volcanic eruptions around the Cretaceous–Paleogene boundary, Palaeogeogr. Palaeocl., 478, 139–148,
715   https://doi.org/10.1016/j.palaeo.2016.05.028, 2017.

Ullmann, C. V., Campbell, H. J., Frei, R., Hesselbo, S. P., Pogge von Strandmann, P. A. E., and Korte, C.: Partial diagenetic overprint of Late Jurassic belemnites from New Zealand: Implications for the preservation potential of δ^7Li values in calcite fossils, Geochim. Cosmochim. Ac., 120, 80–96, https://doi.org/10.1016/j.gca.2013.06.029, 2013.

720

Vandenberghe, N., Craen, M. D., and Beerten, K.: Geological framework of the Campine Basin, SCK• CEN, 112, 2014.

van der Ham, R. W. J. M., van Konijnenburg-van Cittert, J. H. A., Jagt, J. W. M., Indeherberge, L., Meuris, R., Deckers, M. J. M., Renkens, S., and Laffineur, J.: Seagrass stems with attached roots from the type area of the Maastrichtian Stage (NE
725   Belgium, SE Netherlands): Morphology, anatomy, and ecological aspects, Rev. Palaeobot. and Palyno., 241, 49–69, https://doi.org/10.1016/j.revpalbo.2017.02.001, 2017.

van Hinsbergen, D. J., de Groot, L. V., van Schaik, S. J., Spakman, W., Bijl, P. K., Sluijs, A., Langereis, C. G., and Brinkhuis, H.: A paleolatitude calculator for paleoclimate studies. PloS ONE, 10, 2015.

730

Vellekoop, J., Sluijs, A., Smit, J., Schouten, S., Weijers, J. W. H., Sinninghe Damste, J. S., and Brinkhuis, H.: Rapid short-term cooling following the Chicxulub impact at the Cretaceous-Paleogene boundary, Proceedings of the National Academy of Sciences, P. Natl. Acad. Sci. USA, 111, 7537–7541, https://doi.org/10.1073/pnas.1319253111, 2014.

735 Vellekoop, J., Esmeray-Senlet, S., Miller, K. G., Browning, J. V., Sluijs, A., Schootbrugge, B. van de, Damsté, J. S. S., and Brinkhuis, H.: Evidence for Cretaceous-Paleogene boundary bolide "impact winter" conditions from New Jersey, USA, Geology, 44, 619–622, https://doi.org/10.1130/G37961.1, 2016.

Vellekoop, J., Sluijs, A., Speijer, R.P.: An acme of the dinoflagellate cyst Palynodinium grallator, Gocht, 1970; a marker for 740 the late Maastrichtian warming event at Northern mid-latitudes?, Geol. Belg. [accepted manuscript], 2018.

Vellekoop, J., Woelders, L., Sluijs, A., Miller, K. G., and Speijer, R. P.: Phytoplankton community disruption caused by latest Cretaceous global warming, Biogeosciences, 16, 4201–4210, https://doi.org/10.5194/bg-16-4201-2019, 2019.

745 Vellekoop, J., van Tilborgh, K. H. V., Knippenberg, P. V., Jagt, J. W. M., Stassen, P., Goolaerts, S., and Speijer, R. P.: Type-Maastrichtian gastropod faunas show rapid ecosystem recovery following the Cretaceous–Palaeogene boundary catastrophe, Palaeontology, 63, 349–367, https://doi.org/10.1111/pala.12462, 2020.

Vellekoop, J., Kaskes, P., Sinnesael, M., Dehais, T., Huygh, J., Jagt, J., Speijer, R. P., Claeys, P.: A new chemostratigraphic 750 framework for the Maastrichtian type area (southeastern Netherlands, northeastern Belgium), in prep.

Voigt, S., Wilmsen, M., Mortimore, R. N., Voigt, T.: Cenomanian palaeotemperatures derived from the oxygen isotopic composition of brachiopods and belemnites: evaluation of Cretaceous palaeotemperature proxies. Int. J. Earth Sci., 92, 285–299, https://doi.org/10.1007/s00531-003-0315-1, 2003.

755

Watkins, D. K. and Self-Trail, J. M.: Calcareous nannofossil evidence for the existence of the Gulf Stream during the late Maastrichtian, Paleoceanography, 20, https://doi.org/10.1029/2004PA001121, 2005.

Wilf, P., Johnson, K. R., and Huber, B. T.: Correlated terrestrial and marine evidence for global climate changes before mass
760 extinction at the Cretaceous-Paleogene boundary, P. Natl. Acad. Sci. USA, 100, 599–604, https://doi.org/10.1073/pnas.0234701100, 2003.

Winkelstern, I. Z. and Lohmann, K. C.: Shallow burial alteration of dolomite and limestone clumped isotope geochemistry, Geology, 44, 467–470, https://doi.org/10.1130/G37809.1, 2016.

765

Woelders, L., Vellekoop, J., Kroon, D., Smit, J., Casadío, S., Prámparo, M. B., Dinarès-Turell, J., Peterse, F., Sluijs, A., Lenaerts, J. T. M., and Speijer, R. P.: Latest Cretaceous climatic and environmental change in the South Atlantic region, Paleoceanography, 32, 466–483, https://doi.org/10.1002/2016PA003007, 2017.

770 Woelders, L., Vellekoop, J., Weltje, G. J., de Nooijer, L., Reichart, G.-J., Peterse, F., Claeys, P., and Speijer, R. P.: Robust multi-proxy data integration, using late Cretaceous paleotemperature records as a case study, Earth Planet. Sci. Lett., 500, 215–224, https://doi.org/10.1016/j.epsl.2018.08.010, 2018.

Zhang, L., Wang, C., Wignall, P. B., Kluge, T., Wan, X., Wang, Q., and Gao, Y.: Deccan volcanism caused coupled pCO2
775 and terrestrial temperature rises, and pre-impact extinctions in northern China, Geology, 46, 271–274, https://doi.org/10.1130/G39992.1, 2018.

Zhang, J. Z., Petersen, S. V., Winkelstern, I. Z., Lohmann, K. C.: Seasonally variable aquifer discharge and cooler climate in Bermuda during the Last Interglacial revealed by subannual clumped isotope analysis, Paleoceanogr. Paleoclimatol.
780 [accepted manuscript], https://doi.org/10.1029/2020PA004145, 2021.

Zhao, M., Ma, M., He, M., Qiu, Y., Liu, X.: Evaluation of the four potential Cretaceous-Paleogene (K-Pg) boundaries in the Nanxiong Basin based on evidences from volcanic activity and paleoclimatic evolution, Sci. China Earth Sci., 64, 631–641, https://doi.org/10.1007/s11430-020-9736-0, 2021.

785

Zijlstra, J. J. P.: The sedimentology of upper Maastrichtian shelf carbonates in quarry ENCI (Maastricht, The Netherlands). 9th IAS Regional Meeting, Belgium, Excursion Guide 29 [unpublished], 1988.

Zijlstra, J. J. P.: Sedimentology of the Late Cretaceous and Early Tertiary (tuffaceous) chalk of northwest Europe, PhD
790 thesis, Utrecht University, Netherlands, 184 pp., ISBN 90-71577-73-2, 1994.